crystals

MDPI

Article

Formation and Morphological Transition of Diversified Eutectic Structures in Ag-Based Brazing Filler Metals with Sn Addition

Zongye Ding [1,2], Weimin Long [2,3,*], Yongtao Jiu [2,3], Sujuan Zhong [2], Danqing Jiang [4], Chuan Liu [1], Jingwei Yang [1] and Jian Qiao [1,5,*]

1 School of Mechatronic Engineering and Automation, Foshan University, Foshan 528225, China
2 State Key Laboratory of Advanced Brazing Filler Metals & Technology, Zhengzhou Research Institute of Mechanical Engineering Co., Ltd., Zhengzhou 450001, China
3 China Innovation Academy of Intelligent Equipment (Ningbo) Co., Ltd., Ningbo 315700, China
4 State Key Laboratory of Advanced Special Steel, Shanghai University, Shanghai 200444, China
5 Ji Hua Laboratory, Foshan 528200, China
* Correspondence: longweimin@camsouth.com.cn (W.L.); qiaoj@fosu.edu.cn (J.Q.)

Abstract: Eutectic structures in Ag-based brazing filler metals play an important role in improving the properties of alloys and brazed joints. The typical microstructures and morphological evolution of Ag-Cu eutectic structures in Ag-based brazing filler metals solidified at various cooling rates and with the addition of different Sn contents were investigated. The formation mechanisms of anomalous eutectic structure (AES) and the morphological transition from lamellar eutectic structure (LES) to AES were elucidated. The microstructures in alloys solidified at a slow cooling rate and with low Sn content consisted of the full AES, which was attributed to the remelting of the LES during recalescence. Increasing the Sn content and cooling rate promoted the formation of developed Ag dendrite, eutectic dendrite with branches, and AES with large dimensions. The AES in rapidly solidified filler metals with a high Sn content was ascribed to the decomposition of the Ag-rich dendrite skeleton and the growth of Cu-rich between the ternary dendrite arms.

Keywords: Ag-based brazing filler metal; solidification; eutectic structure; morphology

Citation: Ding, Z.; Long, W.; Jiu, Y.; Zhong, S.; Jiang, D.; Liu, C.; Yang, J.; Qiao, J. Formation and Morphological Transition of Diversified Eutectic Structures in Ag-Based Brazing Filler Metals with Sn Addition. *Crystals* **2023**, *13*, 68. https://doi.org/10.3390/cryst13010068

Academic Editor: Xiaochun Li

Received: 30 November 2022
Revised: 23 December 2022
Accepted: 24 December 2022
Published: 31 December 2022

1. Introduction

Due to their low melting point and good performance, Ag-based brazing filler metals containing cadmium have been widely used to produce a brazed joint with good bonding strength and high reliability in the aerospace, electronic information and automobile industries [1–5]. The inherent toxicity of cadmium and environmental protection promote AgCuZn filler metals with the addition of Sn as a substitute for Ag-based brazing filler metals containing cadmium. The addition of a Sn alloying element obviously decreases the solidus and liquidus temperatures of the brazing filler metals and improves the wettability of melt, further optimizing the microstructure and properties of Ag-based brazing filler metals [6,7]. It is worth noting that the Ag-Cu eutectic structure is one of the typical structures in brazing filler metals and brazed joints. The dispersion and morphology of the Ag-Cu eutectic structure have a strong influence on the properties of brazing filler metals and brazed joints. Therefore, it is crucial to investigate the effect of Sn alloying elements on eutectic structures, further controlling the microstructures and improving the performance of brazed joints.

Previous studies regarding Ag-Cu eutectic structures focused on the morphological transition from regular eutectic structures to anomalous eutectic structures (AESs) in Ag-Cu binary alloys after solidification using different undercooling [6–10]. Different eutectic structures exhibit various morphologies, which result in diversified properties of the alloys. It is of significance to elucidate the formation and morphological transition of the different eutectic structures to improve the performance of Ag-based brazing filler metals and

brazed joints. In the undercooled Ag-Cu eutectic alloy, the AES exists adjacent to the nucleation point and changes to a cellular eutectic structure away from the nucleation site with a spasmodic growth pattern [8]. When the undercooling is lower than 70 K, the large composition difference and thermal diffusion coefficient promotes the cellular growth of a lamellar eutectic structure (LES). With increased undercooling, part of the LES remelts and ripens into an AES, and the area of AES increases. When the undercooling is higher than 70 K, the eutectic morphology transforms from cellular to dendritic growth at a high growth velocity [9,10]. For the mechanisms of eutectic lamellar destabilization, the AES formation under an undercooling lower than 72 K is attributed to the termination migration driven by interfacial energy, leading to the destabilization of the LES with a slow eutectic-cellular growth. The AES under an undercooling above 72 K is ascribed to the unstable perturbation of the interface and solute superstation [11]. Additionally, AES formation was reported to be related to increasing the initial undercooling and remelting of the primary LES [12]. For Ag-based brazing filler metals, Ag-Cu eutectic structures with diversified morphologies were found in Ag-based brazing filler metals and brazed joints [13–16]. However, the morphological evolution and formation mechanism of Ag-Cu eutectic structures in Ag-based filler metals with the addition of Sn contents under different conditions is still unclear.

In this study, the morphologies of Ag-Cu eutectic structures in Ag-based brazing filler metals with the addition of different Sn contents and under various cooling velocities were investigated. The morphological evolution under different conditions was determined, and the formation mechanisms of AES and the LES-fibrous eutectic structure (FES) transitions in solidified filler metals were elucidated.

2. Materials and Methods

Pure Ag (99.99 wt.% purity), pure Cu (99.99 wt.% purity) and pure Sn (99.99 wt.% purity) were melted in a medium frequency furnace, then cast into a Cu mold to fabricate Ag-Cu eutectic alloys containing different contents of the Sn alloying element. The chemical compositions of the alloys were characterized using energy dispersive spectroscopy (EDS) analysis; the results are listed in Table 1.

Table 1. Chemical compositions of the cast Ag-Cu alloys (wt.%).

Sample	Alloy Elements		
	Ag	**Cu**	**Sn**
1	71.9	28.1	0
2	71.4	28.1	0.5
3	70.9	28.1	1
4	68.9	28.1	3
5	66.9	28.1	5

To determine the effect of cooling rates and Sn contents on Ag-Cu eutectic structures, samples with the dimension of 5 mm × 5 mm × 5 mm were heated to 1073 K in a high-temperature furnace produced by Gonghui Metallurgical Ltd. under a heating rate of 20 K/s and held for 10 min in an atmosphere of Ar. Next, samples were cooled in the furnace, air, silicone oil and water to room temperature with different cooling rates of approximately 0.1 K/s, 1 K/s, 10 K/s and 30 K/s, respectively. The morphological variation as a function of Sn content and cooling rate was obtained. For the microstructural characterization, specimens were mounted with hot setting powder in a hot mounting press, sanded with different silicon carbide sandpapers (400#, 800# and 1000#) provided by Feili Co., Ltd., and polished to remove surface scratches using the Aachen Polishing Machine. Finally, the microstructure and eutectic morphologies of the various Ag-Cu alloys after solidification under different cooling rates were observed using Phenom scanning electron microscopy (SEM).

3. Results

3.1. Solidification Microstructure

Figure 1 shows the diversified microstructures in the binary Ag-Cu eutectic alloys after solidification at different cooling rates. The bright phase is the Ag-rich crystal, and the dark phase is the Cu-rich crystal. For the Ag-Cu alloy solidified at a cooling rate of 0.1 K/s, the lamellar eutectic structure (LES), Ag dendrite, anomalous eutectic structure (AES) and eutectic dendrite with branches were observed in the sample. The AES crystals were at the boundaries of the LES crystals and/or eutectic dendrites, as shown in Figure 1a. When the cooling rate was increased to 1 K/s, eutectic dendrites were replaced by the columnar eutectic, which was composed of LES and FES. Ag dendrites developed with secondary dendrite arms, and there was a small amount of AES located in the boundary of the columnar eutectic (Figure 1b). With increasing cooling rates, the developed Ag dendrites had tertiary dendrite arms. The microstructure mainly consisted of LES, and a small amount of AES located at the boundaries of the columnar eutectic (Figure 1c). At a cooling rate of 30 K/s, the size of Ag dendrite with developed tertiary dendrite arms increased. Some Cu-rich particles precipitated in the tertiary dendrite arms; the AES crystal was formed at the boundaries of the eutectic dendrites with branches, as shown Figure 1d.

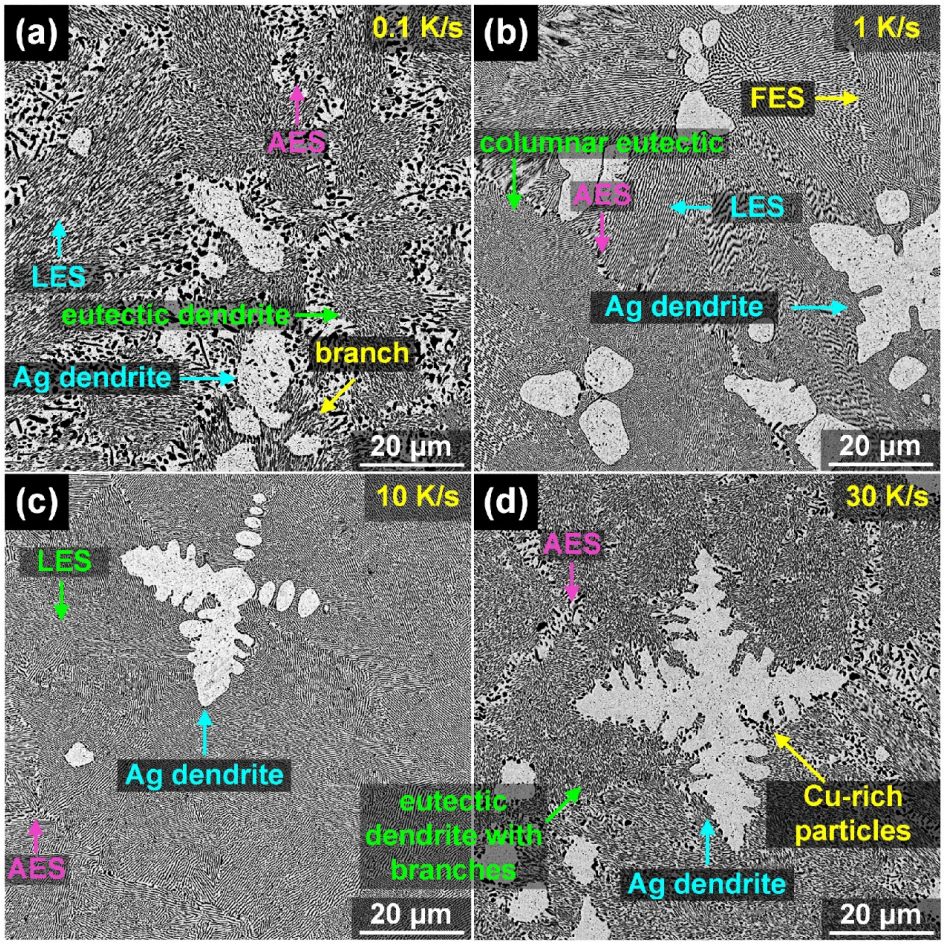

Figure 1. Solidified microstructures in Ag-Cu eutectic alloys under different cooling rates: (**a**) 0.1 K/s, (**b**) 1 K/s, (**c**) 10 K/s and (**d**) 30 K/s.

Figure 2 shows the eutectic growth morphologies developed in the solidified samples with various Sn contents at a cooling rate of 0.1 K/s. After the addition of low Sn content (0.5%), the Ag-Cu eutectic structure consisted of granular and discontinuous Cu-rich particles distributed in the Ag matrix, identified as the full AES, as shown in Figure 2a. When the Sn content was 1%, the Cu-rich particles were continuous, and the dimension

of the Cu-rich phase increased (Figure 2b). With increased Sn content, partial AES was replaced by the newly-fine AES, and the microstructure in the sample was composed of the originally coarse AES and newly-fine AES, as shown in Figure 2c. As the Sn content increased to higher than 5%, the size of the full AES increased, accompanied by discontinuous morphology (Figure 2d). Under a slow cooling rate, the microstructure in Ag-based brazing filler metals mainly consisted of the AES. Increasing the Sn content promoted the continuity and the dimension of the Cu-rich phase in the AES and the formation of new AES.

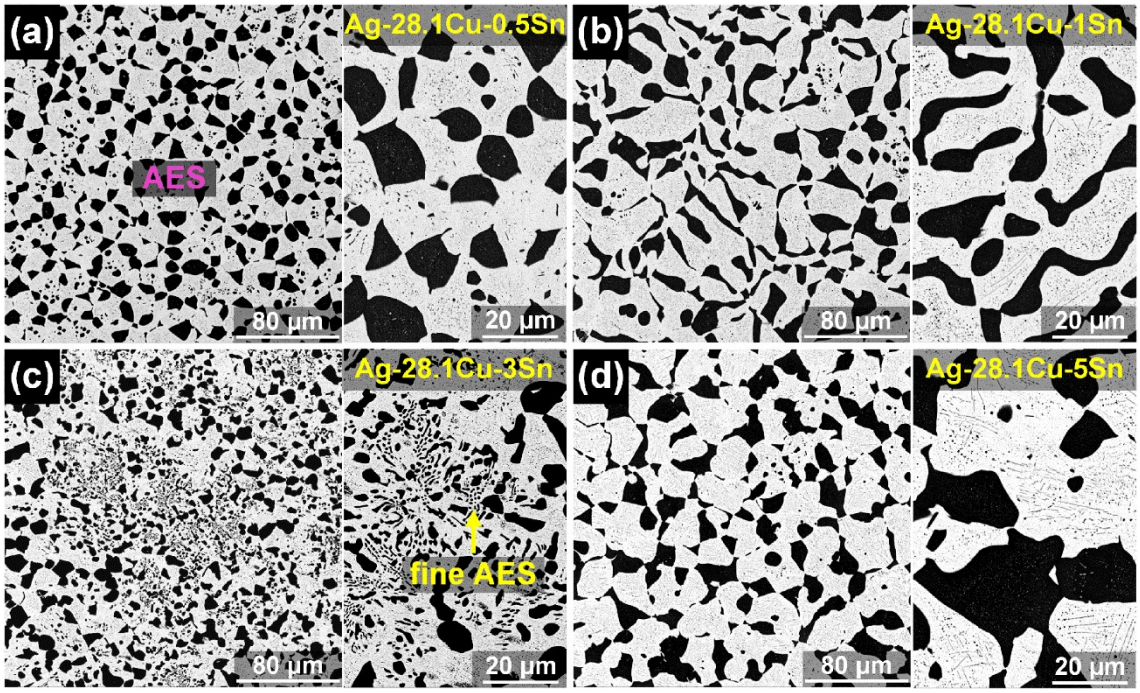

Figure 2. Eutectic morphologies in the Ag-Cu eutectic alloys solidified at 0.1 K/s with different Sn additions: (**a**) Ag-28.1Cu-0.5Sn, (**b**) Ag-28.1Cu-1Sn, (**c**) Ag-28.1Cu-3Sn and (**d**) Ag-28.1Cu-5Sn. Images to the right are magnified images of the Ag-Cu eutectic structures.

The typical microstructures of Ag-Cu eutectic alloys solidified at a cooling rate of 1 K/s with the addition of different Sn contents are shown in Figure 3. For the Ag-28.1Cu-0.5Sn alloy after solidification, the columnar eutectic grains consisted of FES and LES with AES and primary Ag dendrites at the columnar grain boundaries, as shown in Figure 3a. With increasing Sn content, the area of Ag dendrites and AES increased, whereas the amount of FES and LES decreased, accompanied by the morphological transition from LES to FES and the formation of eutectic dendrites (Figure 3b). When the Sn content was higher than 3%, the area of primary Ag dendrite and AES obviously increased, whereas the LES and FES decreased sharply. There were irregular Cu-rich phases formed in the spaces between the adjacent secondary arms, as shown in Figure 3c. As the Sn content increased to 5%, the Ag dendrites continuously increased, accompanied by the formation of many AESs located between the secondary dendrite arms and in the Ag-rich matrix. The LES was greatly reduced with a small amount of FES, as shown in Figure 3d. Therefore, the microstructure in Ag-based brazing filler metal under a cooling rate of 5 K/s was composed of the Ag dendrite, LES, FES, AES at the columnar grains, and AES located in the Ag dendrite and between the secondary arms of Ag dendrites. The increased Sn content enhanced the size of the Ag dendrite and the formation of AES crystals and eutectic dendrite with branches, and decreased the amount of FES and LES crystals.

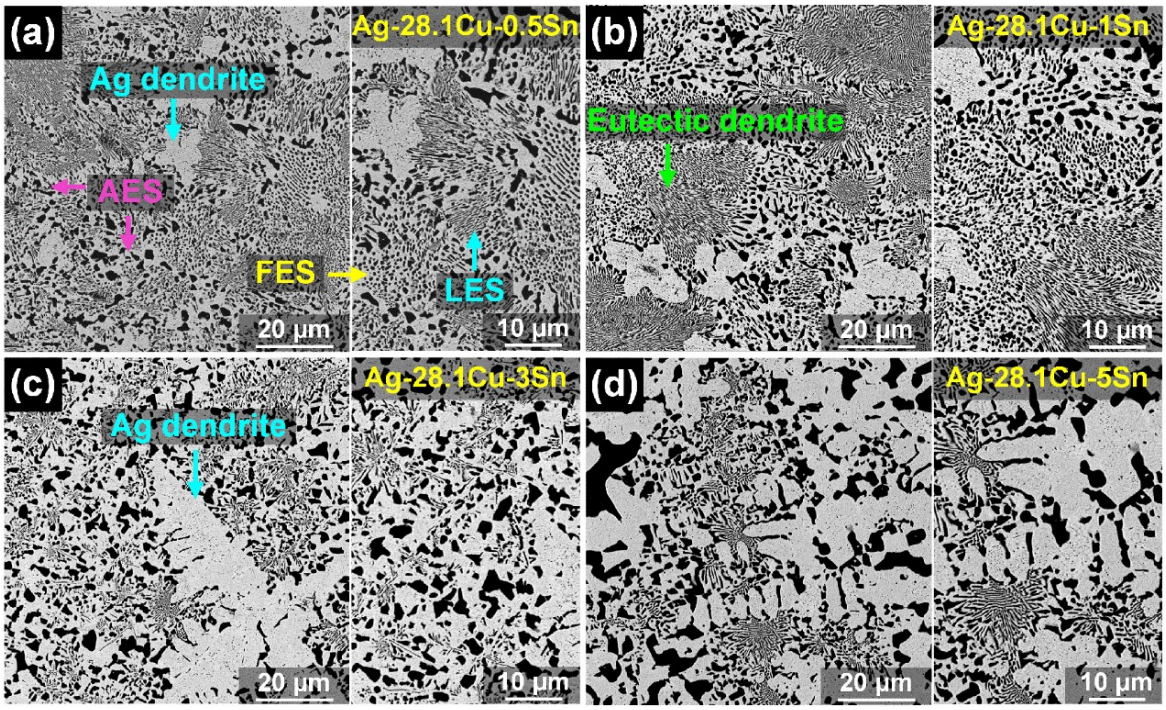

Figure 3. Eutectic morphologies in the Ag-Cu eutectic alloys solidified at 1 K/s with different Sn additions: (**a**) Ag-28.1Cu-0.5Sn, (**b**) Ag-28.1Cu-1Sn, (**c**) Ag-28.1Cu-3Sn and (**d**) Ag-28.1Cu-5Sn.

Figure 4 shows the microstructural morphologies in Ag-Cu-Sn alloys with various Sn contents at the cooling rate of 10 K/s. Ag dendrites, LES, AES, FES, and eutectic dendrites with branches were found in the solidified samples. The AES, eutectic branches and partial Ag dendrites were at the boundaries of the eutectic dendrites, and a few Ag dendrites were in the LES (Figure 4a). The AES and the FES increased with increased Sn content; conversely, the amount and size of LES crystals decreased. Ag dendrites developed and an AES formed in the Ag matrix and between the secondary arms of Ag dendrites, as shown in Figure 4b. When the Sn content was higher than 3%, the microstructure consisted of full AES. The dimension of the Cu-rich particles in the AES increased as the Sn content increased, accompanied by the precipitation of a Cu-rich phase along the Ag grains (Figure 4c,d).

The typically solidified microstructures of the Ag-Cu eutectic alloys as the cooling rate increased to 30 K/s, after adding different Sn contents, is illustrated in Figure 5. For the solidified Ag-28.1Cu-0.5Sn alloy, the structure was composed of Ag dendrites, LES, FES, AES, and eutectic dendrites with branches. The AES and the FES were located at the boundaries of the eutectic dendrites (Figure 5a). As the Sn content increased, the AES and eutectic dendrites with branches increased, whereas the LES and the FES decreased, accompanied by the formation of developed Ag dendrites (Figure 5b). When the Sn content was 3%, full AES crystals, including large Cu-rich particles and partial fine Cu-rich particles, were found in the Ag-Cu-Sn alloy (Figure 5c). As the Sn content increased to 5%, the size of the Cu-rich particles in the Ag matrix increased. Additionally, fine and continuous Cu-rich particles were found to precipitate at the Ag grain boundaries, as shown in Figure 5d.

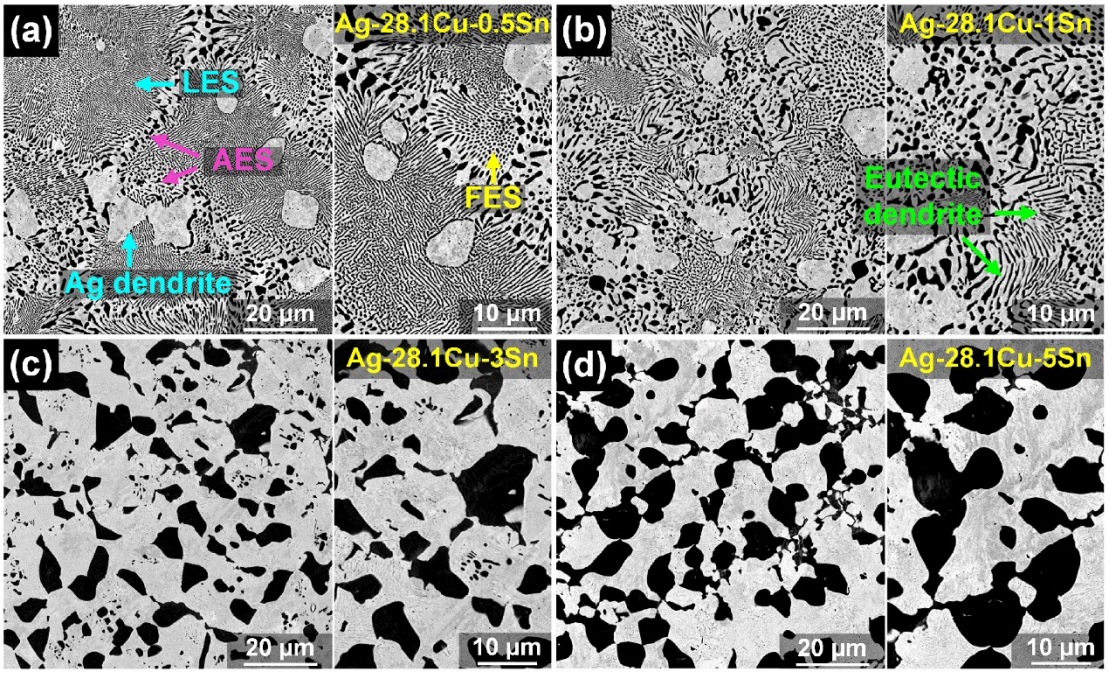

Figure 4. Eutectic morphologies in the Ag-Cu eutectic alloys solidified at 10 K/s with different Sn additions: (**a**) Ag-28.1Cu-0.5Sn, (**b**) Ag-28.1Cu-1Sn, (**c**) Ag-28.1Cu-3Sn and (**d**) Ag-28.1Cu-5Sn.

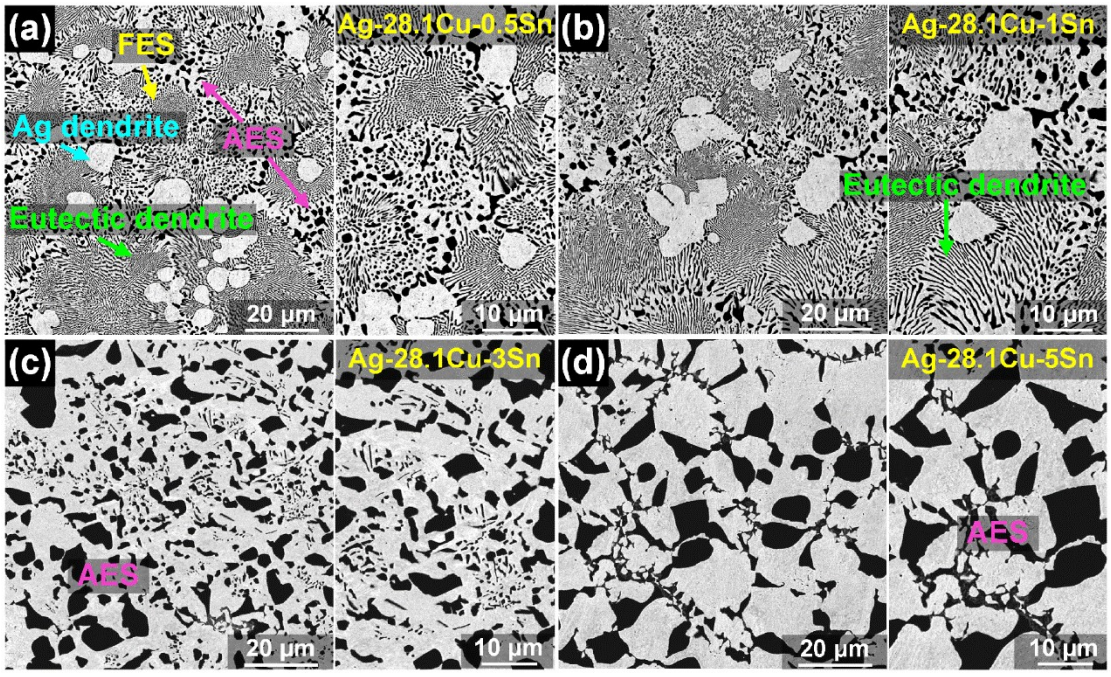

Figure 5. Eutectic morphologies in the Ag-Cu eutectic alloys solidified at 30 K/s with different Sn additions: (**a**) Ag-28.1Cu-0.5Sn, (**b**) Ag-28.1Cu-1Sn, (**c**) Ag-28.1Cu-3Sn and (**d**) Ag-28.1Cu-5Sn.

3.2. Microstructural Map

To determine the effect of cooling rates on the solidified eutectic structures, the microstructural evolution of the Ag-Cu-Sn alloys with different Sn contents and at various cooling rates is illustrated in Figure 6. For the Ag-28.1Cu-0.5Sn and Ag-28.1Cu-0.5Sn alloys, the LES increased with increasing cooling rates, whereas the FES first increased, then decreased. This indicates that the LES gradually transformed into FES and AES. For the

Ag-28.1Cu-3Sn and Ag-28.1Cu-5Sn alloys, the full AES at the slow cooling rate was replaced by the large-scale Ag dendrite and the AES with Cu-rich having an uneven distribution.

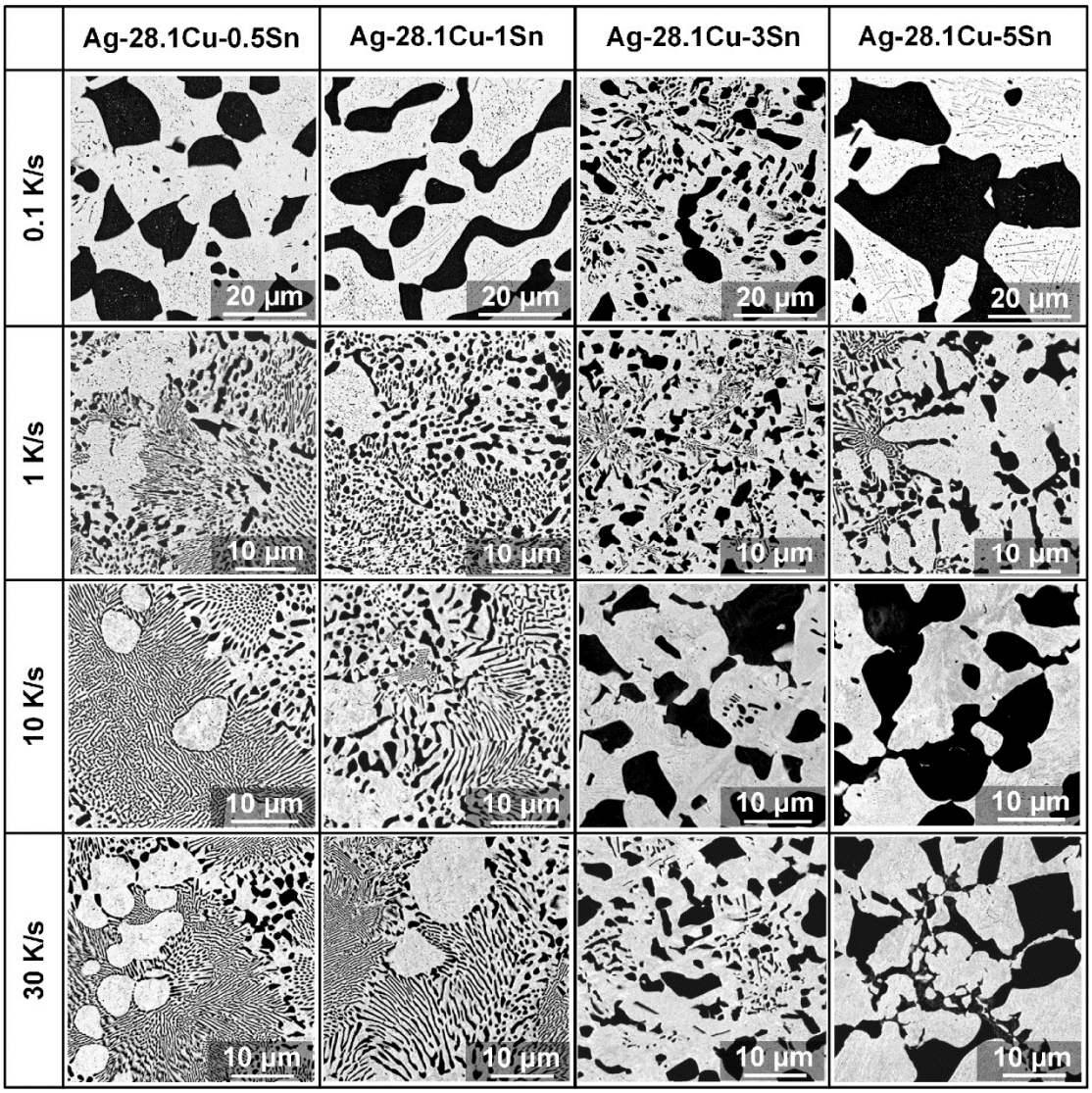

Figure 6. Microstructural evolution of the Ag-Cu eutectic alloys solidified at different cooling rates.

Figure 7 shows the microstructural evolution of the Ag-Cu-Sn alloys with different Sn contents after solidification at various cooling rates. For the Ag-Cu-Sn alloys with low Sn content after solidification at a slow cooling rate, the LES, AES and Ag dendrite were the typical structures in the specimens. With increasing cooling rates and Sn content, the LES transformed into FES and AES, and the solidified structure changed from columnar eutectic to eutectic dendrite with branches. For the Ag-Cu-Sn alloy with a Sn content higher than 3% and solidified at a cooling rate larger than 10 K/s, the microstructure was composed of full AES with a large dimension.

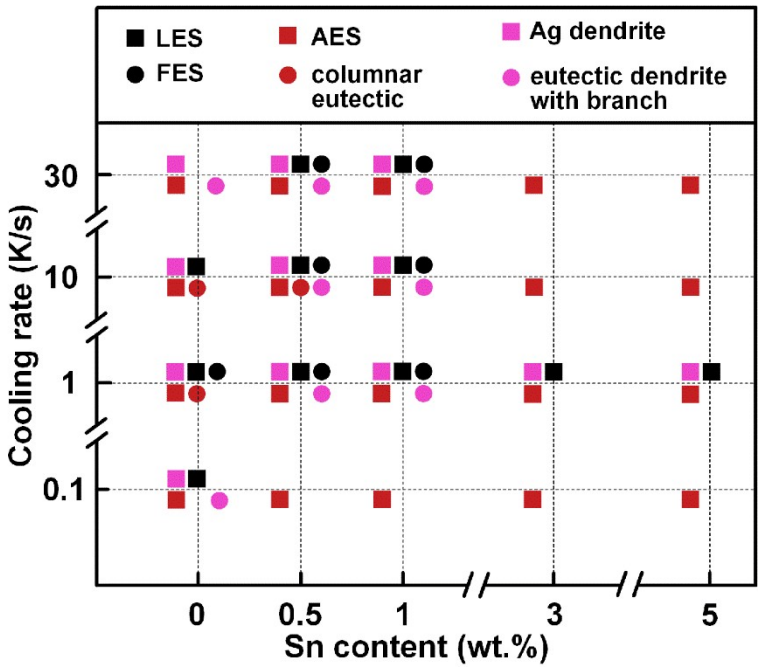

Figure 7. Solidification microstructure map for the Ag-Cu eutectic structures as a function of cooling rate and Sn content. The symbols denote LES (■), AES (■), FES (•), Ag dendrite (■), columnar eutectic (•) and eutectic dendrite with branch (•).

4. Discussion

4.1. LES–FES Transition Mechanism

Figure 8 shows the schematic diagrams of the LES, FES and LES→FES transition. The increased cooling rate and Sn content promoted the transition from the LES to a FES, and the LES and FES growth conformed to the competitive growth model developed by Jackson and Hunt [17].

$$\Delta T_i = K_{1i} V\lambda + K_{2i}/\lambda \tag{1}$$

where $\Delta T_{i=L}$ and $\Delta T_{i=F}$ are the undercooling of the LES and FES interfaces, respectively, K_{1i} and K_{2i} are the relevant constants, λ is the eutectic spacing and V is the growth velocity. The transition criteria for the LES–FES transition requires the conditions based on the minimum LES and FES undercooling and spacing [18].

$$\frac{\Delta T^m_{\mathrm{FES}}}{\Delta T^m_{\mathrm{LES}}} = \sqrt{a f^{n_1}_{\mathrm{Ag-rich}} f^{n_2}_{\mathrm{Cu-rich}} S_{\mathrm{FES}}/S_{\mathrm{LES}}} \tag{2}$$

$$\frac{\lambda^m_{\mathrm{FES}}}{\lambda^m_{\mathrm{LES}}} = \sqrt{b f^{n_3}_{\mathrm{Ag-rich}} f^{n_4}_{\mathrm{Cu-rich}} S_{\mathrm{FES}}/S_{\mathrm{LES}}} \tag{3}$$

where $\Delta T^m_{\mathrm{FES}}$ and $\Delta T^m_{\mathrm{LES}}$ are the minimum undercooling for the FES and the LES, respectively, a, b, n_1 and n_2 are the relevant constants, $f_{\mathrm{Ag\text{-}rich}}$ and $f_{\mathrm{Cu\text{-}rich}}$ are the volume fractions of the Ag-rich and Cu-rich phases in the eutectic structure, respectively, and S_{FES} and S_{LES} are the interface energies for the FES and LES interfaces, respectively. For the LES crystals in Figure 8a, the addition of a Sn alloying element enhanced the constitutional undercooling ahead of the eutectic interface [19]. The relationship between the cooling rate (V) and undercooling (ΔT) followed $\Delta T \propto V$, which indicated increased undercooling with the increasing cooling rate [20]. The spacing variation was dominated by the dynamics of instability, which resulted in perturbed LES and FES spacing equal to the wavelength (λ_1) of perturbation in the lamellae thickness direction, as shown in Figure 8b. As $\Delta T^m_{\mathrm{FES}} < \Delta T^m_{\mathrm{LES}}$ and $1.1547\lambda^m_{\mathrm{LES}} < \lambda^m_{\mathrm{FES}}$, the LES transformed into a FES, as shown in Figure 8c.

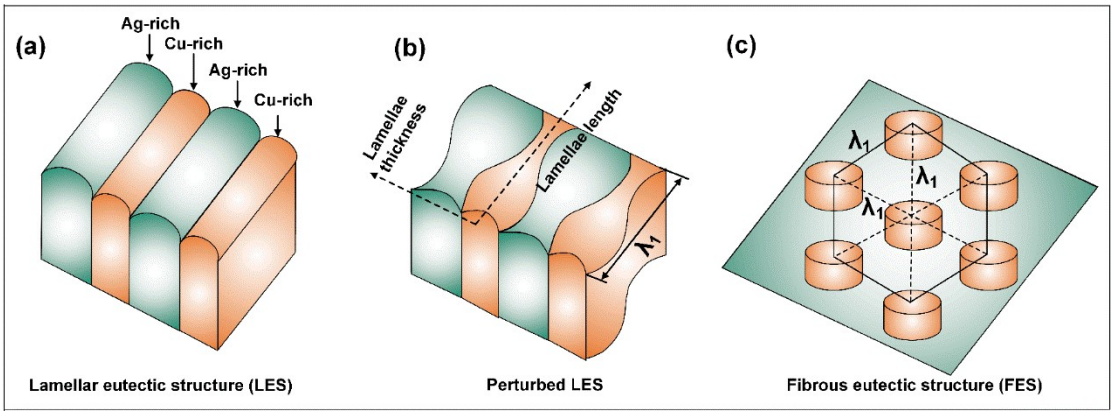

Figure 8. Schematic diagrams of LES (**a**), perturbed LES (**b**) and FES (**c**).

4.2. Formation Mechanisms of AES

For the Ag-28.1Cu-0.5Sn and Ag-28.1Cu-1Sn alloys, the LESs in the rapidly solidified samples indicated that the formation of AES in the Ag-Cu-Sn alloys was ascribed to the remelting of the primary LES; it was directly related to the elevated temperature of recalescence, as shown in Figure 9a. The Cu atomic supersaturation resulting from the trapping effect during solidification promoted the generation of a Cu concentration gradient (ΔC) in the Cu-rich phase of the LES, leading to solute diffusion from trough to peak and the enhanced perturbation of the Cu-rich phase. In addition, capillary force due to the curvature difference created solute/heat diffusion in the Cu-rich phase [21]. The comprehensive effect, including the concentration gradient and curvature difference, enhanced the destabilization of the LES and AES formation during recalescence [22]. For the Ag-28.1Cu-3Sn and Ag-28.1Cu-5Sn alloys, the AESs resulted from primary Ag-rich dendrite growth, as shown in Figure 9b. The growth of Ag-rich dendrite was controlled by solute diffusion and thermal diffusion. The supersaturated Cu alloying element promoted the partial remelting of the tertiary dendrite arms and AES formation during recalescence. At a large undercooling, the dendrite skeleton of the Ag-rich phase divided into several different particles, followed by the nucleation and growth of a Cu-rich phase in the space between the adjacent tertiary dendrite arms and at the boundaries of the adjacent Ag-rich particles. The remelting of primary Ag-rich dendrite and the growth of Cu-rich led to the formation of an AES with large dimension.

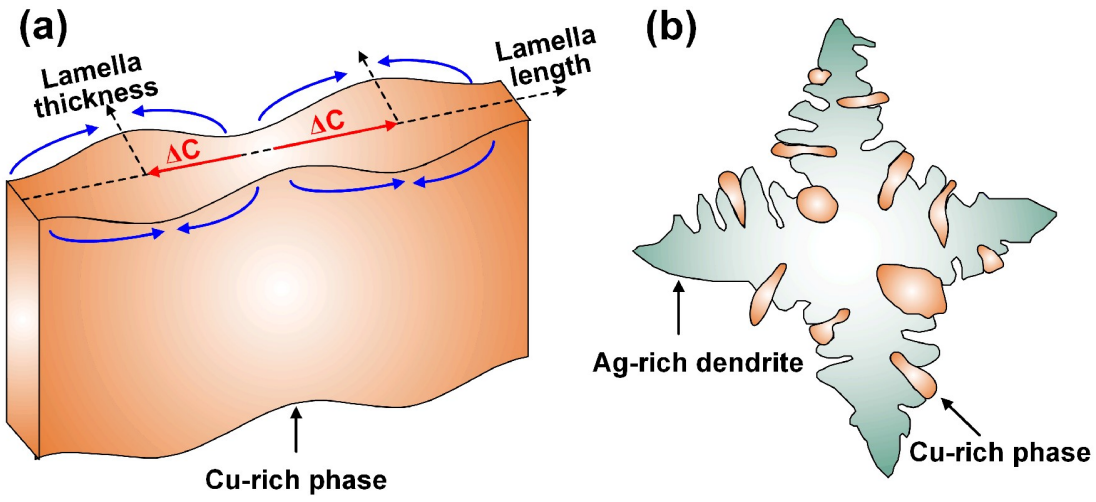

Figure 9. (**a**) Schematic diagram of the AES formation of the Ag-28.1Cu-0.5Sn and Ag-28.1Cu-1Sn alloys and (**b**) schematic diagram of the AES formation of the Ag-28.1Cu-3Sn and Ag-28.1Cu-5Sn alloys.

The eutectic dendrite with branches was one of the typical structures in Ag-based brazing filler metals with the addition of a Sn alloying element. The formation mechanism was attributed to the solute redistribution of the ternary Sn alloying element on the enhancing constitutional undercooling in the melt. The morphological instability of the LES interface was induced and the interfacial morphology was oscillatory, resulting in the transition from the FES to the eutectic dendrite with branches [23].

5. Conclusions

The effects of Sn content and cooling rate on Ag-Cu eutectic structures and their morphological evolution were investigated. Increasing the Sn content and cooling rate enhanced undercooling, which further promoted the LES–FES transition, the formation of AESs and eutectic dendrite with branches. The LES–FES transition resulted from the enhanced constitutional undercooling and perturbed LES dominated by the dynamics of instability. For the alloys solidified at a slow cooling rate and with low Sn content, AES formation was attributed to the destabilization and remelting of the primary LES during recalescence. The formation of AES in the alloys was ascribed to the decomposition of the Ag-rich dendrite skeleton and the growth of a Cu-rich phase in the space between the adjacent tertiary dendrite arms and at the boundaries of the adjacent Ag-rich particles. This provides an in-depth insight into the microstructural evolution and formation mechanisms of diversified Ag-Cu eutectic structures in Ag-based brazing filler metals under different conditions, and further promotes control of the interfacial structure and properties of brazed joints.

Author Contributions: Conceptualization, C.L.; data curation, D.J.; formal analysis, S.Z. and J.Y.; funding acquisition, W.L.; investigation, D.J.; methodology, Y.J. and J.Y.; project administration, J.Q.; resources, C.L.; supervision, W.L. and S.Z.; visualization, J.Q.; writing—original draft, Z.D.; writing—review and editing, Z.D. All authors have read and agreed to the published version of the manuscript.

Funding: This research was funded by the National Natural Science Foundation of China (No. 51904187); the China Postdoctoral Science Foundation (No. 2022M712919), the Open Project of the State Key Laboratory of Advanced Brazing Filler Metals and Technology (SKLABFMT-2021-03), the Science and Technology Program of Guangdong Province (X220391TH220) and the Scientific Research Project of the Education Department of Guangdong Province (2022KCXTD029, 2022KTSCX125).

Conflicts of Interest: The authors declare no conflict of interest.

References

1. Long, W.M.; Zhang, G.X.; Zhang, Q.K. In situ synthesis of high strength Ag brazing filler metals during induction brazing process. *Scripta Mater.* **2016**, *110*, 41–43. [CrossRef]
2. Luo, Q.C.; Xue, S.B.; Wu, J. Influences of Sn on properties of Ag-based and Cu-based brazing filler metals. *Crystals* **2021**, *11*, 1403. [CrossRef]
3. Long, W.M.; Lu, Q.B.; Zhong, S.J.; Qin, J.; Yu, H.; Wu, A.P. Research on interface structure and performance of diamond brazed coating based on non-vacuum environment. *Weld. World* **2022**, *66*, 1043–1052. [CrossRef]
4. Siqueira, L.O.; Silva, A.C.; Marques, I.J.; Gonzalez, C.H.; Santos, T.F. Microstructural evaluation of copper brazed joints using silver-based filler metal. *Metallogr. Microstruct. Anal.* **2021**, *10*, 174–183. [CrossRef]
5. Nishida, T.; Kimura, K.; Inagaki, M. Behavior of Cadmium on Brazing. *Quart. J. Jpn. Weld. Soc.* **1994**, *12*, 485–494. [CrossRef]
6. Watanabe, T.; Yanagisawa, A.; Sasaki, T. Development of Ag based brazing filler metal with low melting point. *Sci. Technol. Weld. Join.* **2011**, *16*, 502–508. [CrossRef]
7. Way, M.; Willingham, J.; Goodall, R. Brazing filler metals. *Int. Mater. Rev.* **2020**, *65*, 257–285. [CrossRef]
8. Clopet, C.R.; Cochrane, R.F.; Mullis, A.M. Spasmodic growth during the rapid solidification of undercooled Ag-Cu eutectic melts. *Appl. Phys. Lett.* **2013**, *102*, 031906. [CrossRef]
9. Zhao, S.; Li, J.F.; Liu, L.; Zhou, Y.H. Cellular growth of lamellar eutectics in undercooled Ag-Cu alloy. *Mater. Charact.* **2009**, *60*, 519–524. [CrossRef]
10. Zhao, S.; Li, J.F.; Liu, L.; Zhou, Y.H. Eutectic growth from cellular to dendritic form in the undercooled Ag-Cu eutectic alloy melt. *J. Cryst. Growth* **2009**, *311*, 1387–1391. [CrossRef]
11. Dong, H.; Chen, Y.Z.; Zhang, Z.R.; Shan, G.B.; Zhang, W.X.; Liu, F. Mechanisms of eutectic lamellar destabilization upon rapid solidification of an undercooled Ag-39.9 at.% Cu eutectic alloy. *J. Mater. Sci. Technol.* **2020**, *59*, 173–179. [CrossRef]

12. Liu, L.J.; Wei, X.X.; Ferry, M.; Li, J.F. Investigation of the origin of anomalous eutectic formation by remelting thin-gauge samples of an Ag-Cu eutectic alloy. *Scripta Mater.* **2020**, *174*, 72–76. [CrossRef]
13. Long, W.M.; Liu, D.S.; Wu, A.P.; Wang, D.C.; Huang, G.Q. Influence of laser scanning speed on the formation property of laser brazing diamond coating. *Diam. Relat. Mater.* **2020**, *110*, 108085. [CrossRef]
14. Zhang, Q.K.; Long, W.M.; Yu, X.Q.; Pei, Y.Y.; Qiao, P.X. Effects of Ga addition on microstructure and properties of Sn-Ag-Cu/Cu solder joints. *J. Alloys Compd.* **2015**, *622*, 973–978. [CrossRef]
15. Sui, F.F.; Long, W.M.; Liu, S.X.; Zhang, G.X.; Bao, L.; Li, H.; Chen, Y. Effect of calcium on the microstructure and mechanical properties of brazed joint using Ag-Cu-Zn brazing filler metal. *Mater. Des.* **2013**, *46*, 605–608. [CrossRef]
16. Wu, J.; Xue, S.B.; Liu, L.; Zhang, P.; Luo, Q.C. Influence of Ga content on the microstructure and mechanical properties of cadmium-free filler metal. *Metals* **2022**, *12*, 1151. [CrossRef]
17. Jackson, K.A.; Hunt, J.D. Lamellar and rod eutectic growth. *Trans. Metall. Soc. AIME* **1966**, *236*, 1129–1142.
18. Liu, S.; Lee, J.H.; Trivedi, R. Dynamic effects in the lamellar-rod eutectic transition. *Acta Mater.* **2011**, *59*, 3102–3115. [CrossRef]
19. Zhao, S.; Li, J.F.; Liu, L.; Zhou, Y.H. Solidification of undercooled Ag-Cu eutectic alloy with the Sb addition. *J. Alloys Compd.* **2009**, *478*, 252–256. [CrossRef]
20. Xian, J.W.; Belyakov, S.A.; Ollivier, M.; Nogita, K.; Yasuda, H.; Gourlay, C.M. Cu6Sn5 crystal growth mechanisms during solidification of electronic interconnections. *Acta Mater.* **2017**, *126*, 540–551. [CrossRef]
21. Dong, H.; Chen, Y.Z.; Wang, K.; Shan, G.B.; Zhang, Z.R.; Huang, K.; Liu, F. In situ observation of remelting induced anomalous eutectic structure formation in an undercooled Ni-18.7 at.%Sn eutectic alloy. *Scripta Mater.* **2020**, *177*, 123–127. [CrossRef]
22. Clopet, C.R.; Cochrane, R.F.; Mullis, A.M. The origin of anomalous eutectic structures in undercooled Ag-Cu alloy. *Acta Mater.* **2013**, *61*, 6894–6902. [CrossRef]
23. Plapp, M.; Karma, A. Eutectic colony formation: A stability analysis. *Phys. Rev. E* **1999**, *60*, 6865–6889. [CrossRef] [PubMed]